MODELING THE ASR INDUCED STRAINS AND CRACKING OF REINFORCED CONCRETE BEAMS

A Thesis

by

LI ZHANG

Submitted to the Office of Graduate Studies of
Texas A&M University
in partial fulfillment of the requirements for the degree of

MASTER OF SCIENCE

Chair of Committee,	John Mander
Committee Members,	Philip Park
	Mohammad Naraghi
Head of Department,	John Niedzwecki

August 2013

Major Subject: Civil Engineering

ABSTRACT

In the past few decades, several researchers have studied the effects of ASR induced expansion in concrete. Several models have been proposed to model the effects of ASR in concrete. While most of these models focus on plain concrete, there is limited amount of research to model the influence of ASR expansion in reinforced concrete. Additionally, the existing models are complex and difficult to implement for practicing engineers. In this study the shortcomings with the existing models are addressed.

A minimalist semi-empirical model is developed to represent the degradation of reinforced concrete due to ASR expansion. The model is validated using historical experimental data. Only two key parameters are needed to represent the expansive behavior, specifically, the maximum unreinforced concrete strain due to ASR expansion and the rise time. Mechanical properties of the reinforced concrete are also needed.

From the predicted expansions, it is then shown that it is possible to model the number and spacing of cracks of a partly restrained reinforced concrete beam affected by ASR gels. The model is validated with recent experimental results on large scale reinforced concrete specimens. Predictions agree well with the observed number of cracks.

DEDICATION

To My Grandparents, Who Raised Me Up

ACKNOWLEDGEMENTS

I would like to thank my committee chair, Dr. Mander for his invaluable guidance, patience and support throughout the course of this research. This research would not have been possible without his thoughts and financial support.

I would also like to thank my committee members, Dr. Park and Dr. Naraghi for serving on my committee and for their vision and thoughts. I would like to thank my former advisors Dr. Grasley and Dr. Abu Al-Rub when they were at Texas A&M University. Thanks also to the faculty and staff at Texas A&M University for providing the friendly academic atmosphere for study.

I would like to show my gratitude to Madhu Karthik for his friendly suggestions and corrections during this research. Also my appreciation is extended to my friends Yi Yang and Jialiang Wang who helped me through the difficult times during the process of the two year master's study.

Last, but not the least I would like to thank my grandparents who raised me. Thanks are also extended to my father and mother for their constant support.

TABLE OF CONTENTS

Page

Page

LIST OF FIGURES

Page

LIST OF TABLES

Page

1. INTRODUCTION

1.1 Background and Motivation

The durability of concrete structures can be affected by several degradation mechanisms. The degradation mechanisms not only include external factors such as drying, freezing-and-thawing cycles, or sulfatic water, but also include the chemical reactivity in the concrete such as shrinkage and alkali-aggregate reaction swelling. It is known that the most common possible reaction is that between the relatively high alkali content in cement with aggregates containing enough reactive silica. Alkali-Silica Reaction (ASR)-a chemical reaction of the alkalis with the hydrous forms of the silica present in the mineral constituents, defined by Bazănt and Steffens (2000), was first proposed by Santon (1940). Blanks (1941) and Meissner (1941) explained it early. Reactive siliceous products of the Alkali-Silica Reaction (ASR) occur in concrete when alkali from the cement reacts with free silica present in aggregates to form an alkali-silica gel (Tarig et al, 2003). In the presence of moisture, the ASR gel expands, and then exerts pressures on the surrounding concrete matrix over time, thereby causing degradation of concrete structures.

It is known that the conditions required for the occurrence of ASR are as follows: reactive siliceous aggregates, high alkali contents in cement, a transport medium such as water and high temperature. The reaction usually occurs sometime after the concrete is cast. The time depends on several factors. Depending on the extent of reactive particles, a significant volume of ASR gel can form, which absorbs moisture and expands within the hardened concrete, thus resulting in cracks. The problem is quite complex, and the

chemical mechanism is not fully understood. As mentioned earlier, the reaction is influenced by many factors. Several previous attempts have proven that it is quite difficult to develop a comprehensive model that can be used to analyze the realistic response of ASR affected concrete structures based on the present knowledge of the ASR mechanisms.

Hansen (1944) proposed an osmotic pressure theory to explain the mechanism of expansion of certain concrete structures. Later, Dent (1979) applied the theory to the mechanism of ASR induced expansion in concrete structures. Bazănt and Steffens (2000) proposed that the ASR induced expansion in concrete is due to the swelling pressure accumulated in the interfacial transition zone between the aggregate and the surrounding cementitious material. Also, the authors developed macroscopic models to analyze the overall concrete behavior due to ASR at a structural scale.

Most of the authors mentioned above combined the finite element method with the chemical mechanism. Almost all of the work done until now has focused on the deterioration of concrete due to ASR. However a model that is intended for the swelling strain analysis of reinforced concrete structures is necessary for the development of ASR induced degradation in reinforced concrete.

The current work comprises of four sections. Following this introductory section, a literature review is also presented in section 1. The next two sections analyze the effect of ASR gels on reinforced concrete structures. In section 2, through a strain energy approach, a new minimalist semi-empirical model is presented to calculate the ASR induced concrete strain over time. It is validated by the experimental data from other

references (Jones and Clark, 1996 and Hobbs, 1988). In section 3, a mechanical theory to model the number and spacing of cracks of a reinforced concrete beam due to ASR gels is proposed. The theory is also validated against experimental result from Mander et al. (2012). Finally, section 4 provides a summary, specific conclusions and recommendations for further research.

1.2 Problem Statement

Over the past decade, the structural longevity of a large number of reinforced concrete structures has been compromised as a result of premature concrete deterioration that is generally attributed to ASR. ASR plays an important role in the durability of concrete structures. Thus a practicing model which can predict the strain change of a concrete structure under the influence of ASR is in demand. Despite much research being done on this topic, most of them are focused on ASR affected concrete. There are limited investigation and theories developed on degradation of reinforced concrete due to ASR. Also, existing models are heavily based on highly mathematical formulations, and are difficult to implement for practicing engineers. Therefore, a minimalist semi-empirical model is presented which can be applied in real world for engineers.

1.3 Research Objectives

The main objectives of the proposed research project are to:

i. determine maximum expansion due to ASR in reinforced concrete for different reinforcement ratios.

ii. establish a minimalist semi-empirical model capable of estimating the expansion strain caused by ASR on reinforced concrete beam over time. Such

a method can be used for capacity analysis or design of reinforced concrete members in Texas.

iii. analyze stress condition in reinforcement and concrete separately for a partly restrained reinforced concrete beam under the influence of ASR gels.

iv. establish a theoretical model to calculate the number and spacing of cracks in a partly restrained reinforced concrete beam under the influence of ASR gels.

v. identify the influence of different parameters such as tensile stress of concrete $f_t^{'}$ and Young's modulus of concrete E_c on the expansion strains and number of cracks in reinforced concrete structure due to ASR expansion.

1.4 Review of Previous Work

The investigation into the chemical mechanism of ASR and its subsequent influence on concrete structures has been a popular research topic for some time. A brief review of the concept of ASR and the mechanism of expansion is outlined first in this section, and a state-of-the-art of modeling for ASR in plain concrete and reinforced concrete is then presented.

Secondly, work recently published by Mander et al. (2012) is introduced. In this report, the effect of concrete deterioration due to evolving ASR and Delayed Ettringite Formation (DEF) is examined on large-scale specimens that represent typical modern Texas reinforced concrete bridge piers.

1.4.1 ASR Chemistry and Mechanics

Dent and Kataoka (1981) clarified the ideas about the normal ASR chemical reaction. In concrete, the reactive siliceous aggregates and high alkali contents in cement

can induce ASR when exposed to moisture and high temperature. ASR first starts with the dissolution of silica on the surface of the aggregate particles. At the interface of the aggregate and the alkaline solution, Hydroxyl ions react with the two generally poor crystallized silica bonds: the siloxane bonds, Si-O-Si, and the silanol groups, Si-OH. These chemical processes can be represented stoichiometrically as follows:

$$\mathrm{Si-O-Si+OH^- \rightarrow Si-OH+OH-Si} \tag{1.1}$$

$$\mathrm{Si-OH+OH^- \rightarrow SiO^- + H_2O} \tag{1.2}$$

The silanol bonds from (1.1) together with the preexisting ones contained in hydrous silica aggregates, can react with further hydroxyls. In an environment with low calcium ion (Ca^{2+}), the alkaline ions K^+ and Na^+ which are present in the interstitial pore solution can work with the resulting negative charges from (1.2). The mechanisms behind the formation of the expansive reaction products are still unknown. But it seems that the dissolved ions diffuse due to differential spatial concentrations through the pore solution to microvoids, pores, and cracks, forming various reaction productions. This gel formation exerts internal pressure in the cement matrix on the concrete skeleton based on the location and the amount of water.

As the ASR gel starts to form, tensile stresses are imposed internally within the concrete system and this leads to cracking. The hydrated cement paste is generally weaker than the aggregates, hence the cracking usually occurs in the hydrated cement paste or along the interface of the aggregate and the hydrated cement paste. Jensen

(2004) indicated that eventual expansion due to ASR can cause cracking of the aggregates although it initiates in the hydrated cement paste.

Ulm et al. (2000) developed a thermo-chemo-mechanics behavior theory for ASR affected concrete, which is broadly accepted by researchers. The swelling mechanism is plotted in Figure 1-1a. In this model, it is assumed that the macroscopic stress due to external effects is zero, which means the model is under a stress-free condition. As the ASR gels expand over time, the swelling pressure p_g is balanced by the tension σ_μ in the concrete skeleton. Consequently, the entire material swells. The other assumption adopted in this model is that the concrete skeleton is conceived as an elastic material, which can be represented as elastic springs as shown in Figure 1-1b where σ is the external stress from outside, ε is the overall strain in the model, E_m is the stiffness of the elastic spring, and the stress in the elastic spring is represented by $\sigma_\mu = E_m \varepsilon$. p_g is the swelling pressure in the chemical gel, and ξ is the extent of this chemical reaction. Another assumption in this model is that the volume increase of the products is proportional to the reaction extent. The stress equilibrium in this chemoelastic model is as follows:

$$\sigma = \sigma_\mu - p_g = E_s \varepsilon + E_g (\varepsilon - \kappa \xi) \tag{1.3}$$

where

$$\sigma_\mu = E_s \varepsilon ; \quad p_g = -E_g (\varepsilon - \kappa \xi) \tag{1.4}$$

where E_g and E_s are spring modulus.

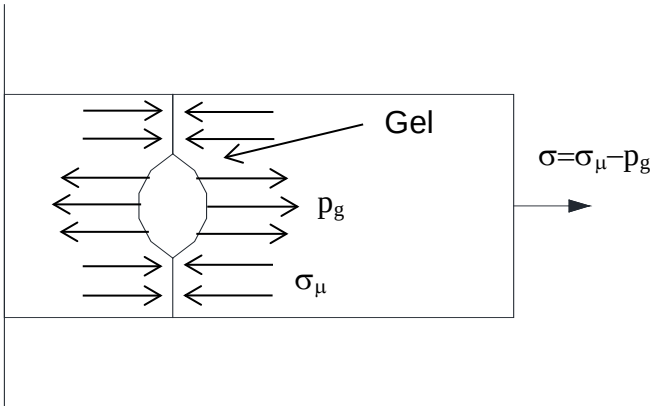

(a) ASR swelling mechanism

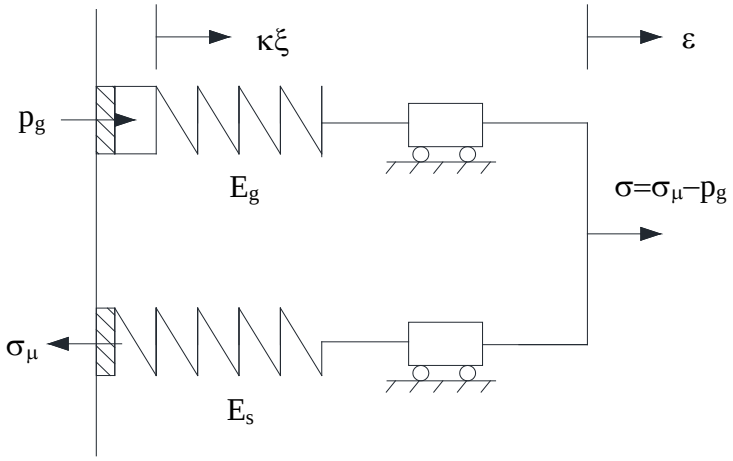

(b) Kinematic model

Figure 1-1: ASR expansion and analog model.

In this case, as a stress-free condition is assumed, (1.3) yields the following:

$$\sigma = 0: \qquad \varepsilon = \beta\xi; \qquad \beta = \frac{\kappa E_g}{E_g + E_s} \tag{1.5}$$

These constitutive equations under stress-free condition provide a direct experimental access to the macroscopic ASR kinetics from stress-free expansion tests.

Furthermore, Ulm et al. (2000) developed a thermodynamically based model for the expansion evolution, as shown in Figure 1-2 and given by the following equation:

$$\varepsilon(t) = \varepsilon(\infty)\xi(t); \qquad \xi(t) = \frac{1 - \exp(-t/\tau_c)}{1 + \exp(-t/\tau_c + \tau_L/\tau_c)} \tag{1.6}$$

where t is the time parameter, τ_L and τ_C are the latency and characteristic times. The latency time corresponds to the inflexion point, and the characteristic time is defined in terms of the intersection of the tangent at τ_L with the asymptotic unit value of ξ. The two coefficients are defined as follows:

$$\begin{aligned} \tau_c(\theta) &= \tau_c(\theta_0)\exp[U_c(1/\theta - 1/\theta_0)] \\ \tau_L(\theta) &= \tau_L(\theta_0)\exp[U_L(1/\theta - 1/\theta_0)] \end{aligned} \tag{1.7}$$

where θ is the temperature, and θ_0 is considered as the temperature where an isothermal stress-free ASR expansion test was done. U_L and U_c are considered as the minimum activation energies required to start the reaction for the latency and characteristic times, respectively, and can be calculated to be as follows:

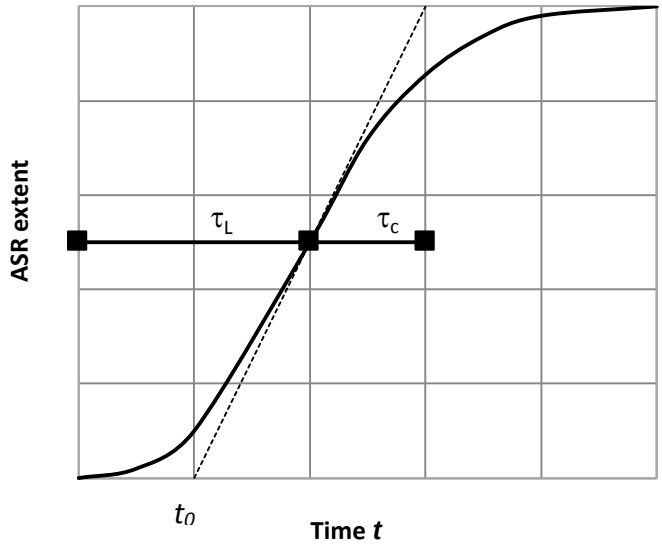

Figure 1-2: Definitions used in previous work.

$$U_L = 9400 \pm 500K$$
$$U_L = 5400 \pm 500K \quad (1.8)$$

Saouma and Perotti (2006) considered the influence of stress on concrete affected by ASR expansion. Relatively high compressive and tensile stresses were assumed to result in the reduction in ASR induced expansion. The reason that the stresses inhibit the reaction extent of ASR can be the formation of microcracks or macrocracks that absorb the expanding ASR gels. Also, two functions in terms of tensile and compression stresses were proposed to account for this reduction. Therefore, ASR expansion strains in the three directions are determined based on the stress state, resulting in anisotropic ASR expansion.

Comi et al. (2009) developed a chemo-thermo–damage model by the combination of the reaction kinetics with an isotropic damage model. In this model, the concrete affected by alkali aggregate reaction is considered as two materials composed of the expanding gel and the concrete skeleton. The gel expansion induced micro-cracking is considered by an isotropic damage model based on the definition of two parameters, one for stress states of tension and the other for compression. Later, considering the effect of temperature and humidity conditions, Comi et al. (2012) implemented the model in a finite element code, which can be applied in the analyses of structures made of reactive concrete under the curing condition in the presence of temperature and moisture gradients.

Besides the models based on thermo-chemo-mechanics, Mukhopadhyay et al. (2006) introduced a concept of ASR-related activation energy which was used as a

representative single parameter for the prediction of ASR. In this model, the only parameter to evaluate ASR extent is the activation energy. Also, a dilameter test method was introduced as part of a performance-based testing protocol for analyzing the ASR aggregate reactivity in terms of the activation energy.

Little attention has been paid to extend the preliminary investigation to examine the progress of the reaction in reinforced concrete. Swamy and Al-Asali (1989), and Fan and Hanson (1998) have emphasized the reduction of the observed ASR-induced strains due to reinforcing bars.

Multon et al. (2006) studied the possibility of modeling ASR expansions as imposed strains that depend on the concrete mix-deisgn and environmental conditions as described in the thermo-chemo-mechanical model developed by Ulm et al. (2000) and Li et al. (1999). In this approach, the required external input data are the temperature and the moisture conditions (determined by in-situ measurements). The ASR-induced strains are computed knowing the potential expansion due to the concrete mix-design.

Pietruszczak and Winnicki (2003) described reinforced concrete as a composite medium comprising concrete mix and reinforcement. Later, Winnicki and Pietruszczak (2008) incorporated the chemo-mechanical interaction associated with continuing ASR. It is noted that the general concept outlined in the above work was similar to the work of Ulm et al. (2000).

1.4.2 Experiments at Texas A&M University on ASR/DEF in Reinforced Concrete

1.4.2.1 Summary

This section summarizes the work recently published by Mander et al. (2012). The effect of concrete deterioration due to evolving ASR and DEF is examined on large-scale specimens that represent typical modern Texas reinforced concrete bridge piers. Specimens are designed and constructed with a special mix that aims at promoting ASR and cured at high temperatures to promote DEF. Following loading, that mimics prototype gravity effects, the specimens have a moderate amount of cracking that permits moisture ingress. The specimens are conditioned outdoors in the Texas heat under daily wetting and drying cycles. Over a two-year period, substantial crack progression due to the effect of ASR/DEF resulted. While map cracking of concrete that indicates the formation of ASR gel is observed at an early age, over time the surface and internal concrete strains as well as reinforcing steel strains show substantial evidence of dilation due to ASR effects. This is also verified using post-test petrographic analysis. Results show that much of the ASR-induced damage is concentrated in the concrete cover, while the reinforcing cage tends to restrain the ASR expansion of core concrete due to its confining effect.

1.4.2.2 Specimen Design

Straddle bents typically have both tension and compression steel in the bent cap to accommodate the alternating negative and positive moments along the cap beam. The

bottom (positive moment) reinforcement needed for the mid-span region of the cap beam is normally terminated inside the column face within the beam-column joint zone.

Figure 1-3 presents the specimen dimensions and the reinforcing details of the C-shaped specimens. The longitudinal reinforcement, scaled to replicate the cantilever and straddle bents described previously, consisted of 10 No.8 rebars (1.0 inch/25 mm diameter) running continuously on the tension side of the specimen and hooked at the end of each bent. The singly reinforced bent cap section (S) had only two No.8 bars on the compression face. These bars are necessary for construction purposes in order to tie the transverse steel and form an enclosed cage. The doubly reinforced bent cap section (D) had 10 No.8 bars in both the tension and compression faces of the beam.

The longitudinal side face bent reinforcement (distributed along the web of bent cap web) consisted of three sets of equally spaced No.4 rebars (0.5 inch/13 mm diameter). Transverse bent cap reinforcement consisted of closed stirrups with a center-to-center spacing of 4.5 inches (115 mm) starting at the column face. The longitudinal column reinforcement, in addition to the 10 No. 8 rebars used in the tension region, consisted of five sets of equally spaced No. 8 rebars throughout the mid-region of the column section and five No.8 rebars along the compression face. Transverse column reinforcement consisted of 4.5 inch center-to-center spaced No.4 overlapping hoops. The beam-column joint was reinforced with four No.4 U-bars with 8 inch spacing continuing from the transverse bent reinforcement.

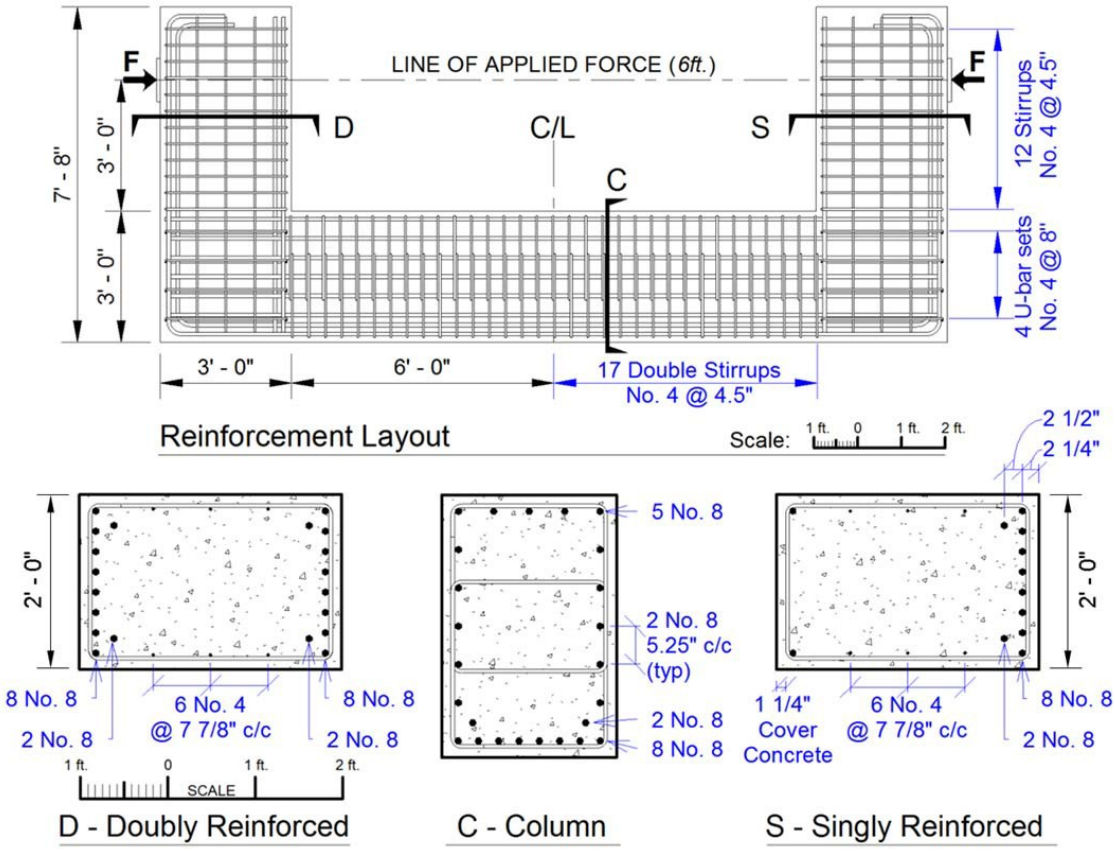

Figure 1-3: Reinforcement details of experimental specimen tested by Mander et al. (2012).

1.4.2.3 Summary of Experimental Specimen Development

Table 1-1 presents a summary of cast date, age when prestress was applied, age at the beginning of wetting and drying cycles, age when specimen was shipped back to the structural testing lab, and age when testing was conducted for each specimen. Note that prestress was removed before the specimens were shipped back to the structural testing lab.

Table 1-1: Summary of experimental specimen development (Mander et al. 2012).

	Lab		***Field***	***Lab***	
	Cast Date	**Prestress Applied**	**Wetting and Drying Cycles**	**Moved to lab with prestress removed**	**Testing**
Specimen		Age (days)	Age (days)	Age (days)	Age (days)
1	11/24/08	N/A	N/A	N/A	392
2	01/13/09	97	112	364	499
3	02/13/09	66	81	-	-
4	03/06/09	45	60	808	888

The specimens were internally heated to maintain the temperature above 170 °F (77 °C) for at least 2 days. The top formwork was removed after shutting off the heat, while the side formwork remained in place for at least 1 day. The beam area of one side of Specimen 4 was thermally shocked immediately after the removal of top formwork.

1.4.2.4 Visual Observation over Time

Figure 1-4a shows the first crack pattern of Specimen 4 at 48 days. In addition to the growth of the load-induced cracks, some new map cracking was noticed over the first 75 days along with some new cracks that aligned themselves with the longitudinal rebars

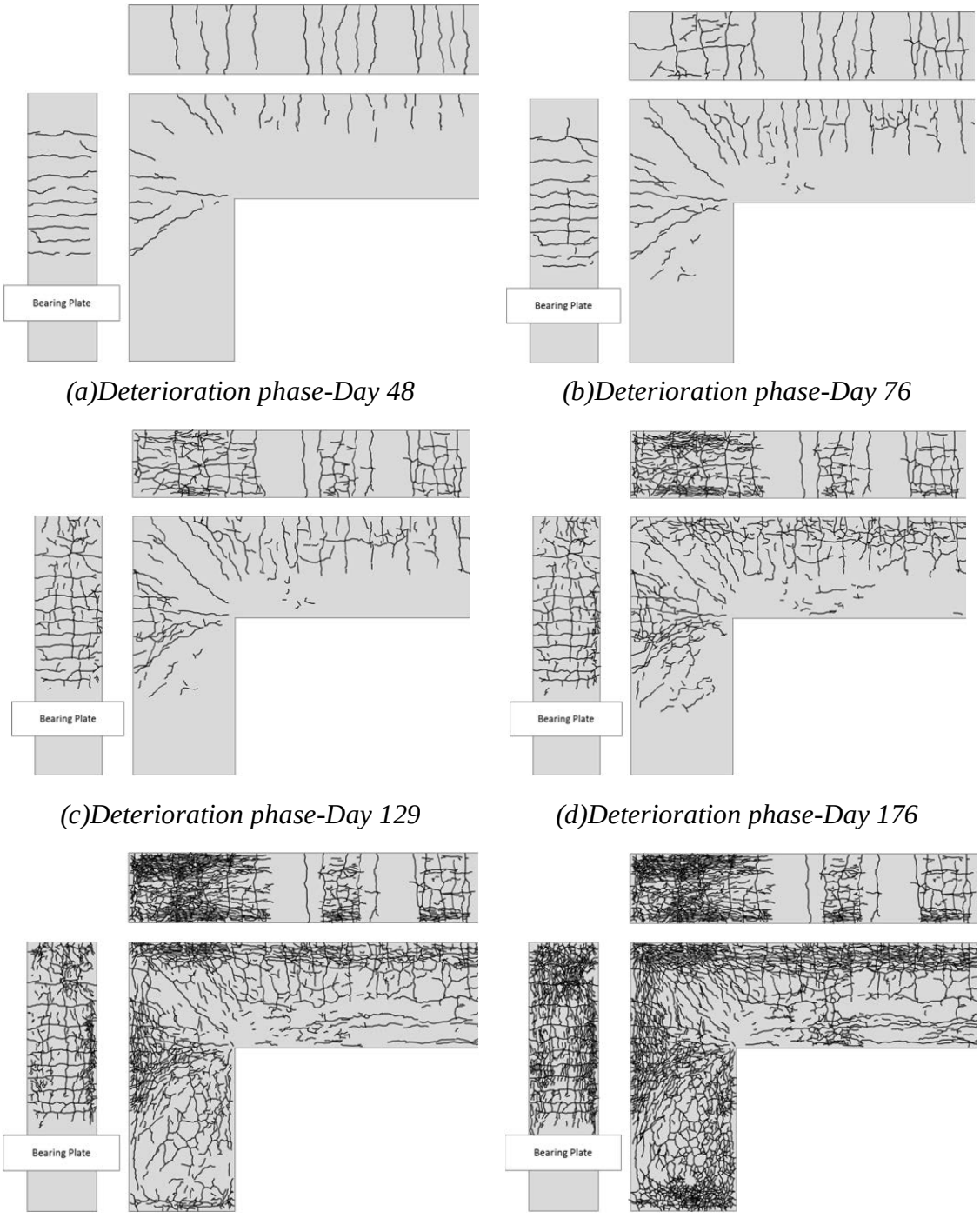

(a)Deterioration phase-Day 48 *(b)Deterioration phase-Day 76*

(c)Deterioration phase-Day 129 *(d)Deterioration phase-Day 176*

(e)Deterioration phase-Day 406 *(f)Deterioration phase-Day 748*

Figure 1-4: Crack pattern observed in C-Beam specimen subjected to cracking due to ASR/DEF effects (Mander et al. 2012).

as shown in Figure 1-4b. The widening of the load-induced cracks provided additional access for the concrete to imbibe moisture.

1.4.2.5 Reinforcing Steel Strains

Figure 1-5 shows the reinforcing steel strains over a two-year period for Specimen 4. Once loaded by the prestress (15 days prior to beginning of the deterioration phase), the strains in the main longitudinal bar were immediately within the range of 0.0005 to 0.0008 (22 to 36 percent of yield strain, Figure 1-5b and c) before the specimens were shipped to the field. The reinforcing strains then gradually increased in the first four months. In the subsequent period, compression strains were recorded. This most likely indicated force re-distribution between the main longitudinal rebars. Also, formation of ASR gel around the rebars may cause de-bonding between the concrete and steel and resulted in local compression strains. Note that there was a longitudinal crack right above the longitudinal rebar that was instrumented with strain gages. This crack possibly introduced more moisture, promoted local formation of ASR gel, and caused the unpredictability of measured reinforcing steel strains. Also, faulty readings may have been recorded due to the development of faulty gages over time from the ASR/DEF deterioration. Note that several gages failed (stopped reading) due to the ASR/DEF deterioration over time. The strain in the hoop steel (gage SG3) gradually increased during the summer and reached the tensile yield strain at about 70 weeks (Figure 1-5d). It is evident that the ASR expansion introduced some confining effect to core concrete and eventually led the hoop steel reach yield strain. It is also evident that the ASR-induced deterioration in the cover concrete would offset any beneficial confining effect

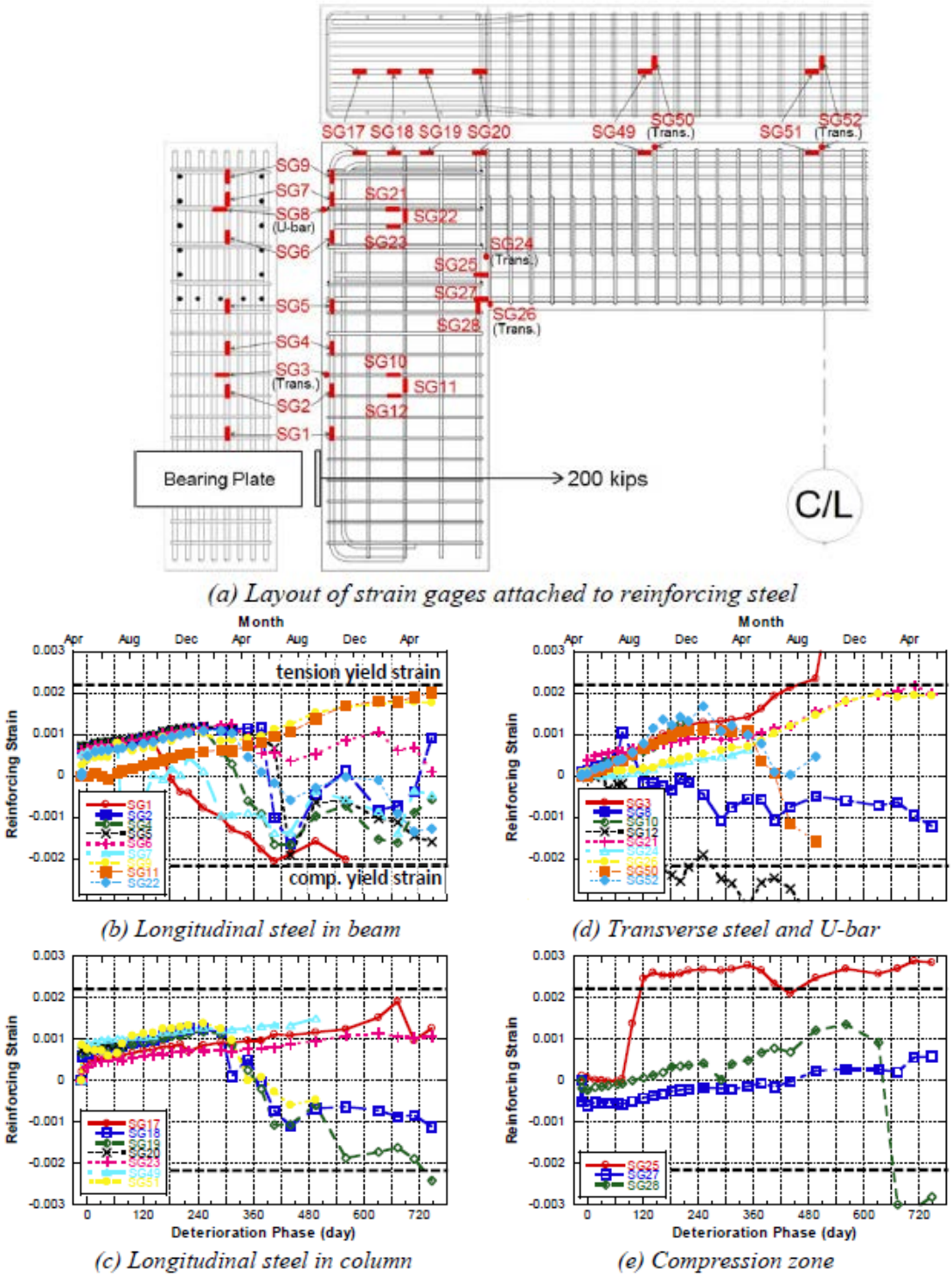

Figure 1-5: Reinforcing steel strain from strain gauges by Mander et al.(2012).

in the core concrete. Due to the unpredictability of the locations of ASR gel formation, other reinforcing strains as recorded appeared to have random patterns (Figure 1-5d and e). This might result from local force re-distribution and debonding between concrete and reinforcing steel.

2. MODELING THE SWELLING STRAINS INDUCED BY ASR EFFECTS IN REINFORCED CONCRETE

2.1 Introduction

In the past, several investigators have developed predictive time-dependent models to analyze the behavior of the swelling strain induced by ASR-effects on plain concrete. These investigators include, but are not limited to Ulm et al. (2000) and Comi et al. (2009). Many of the existing models were formulated in the framework of the finite element method by combining the chemical aspects of ASR with its mechanical effects. Only a few models focusing on the deterioration of reinforced concrete due to ASR, for example, Multon et al. (2006), Winnicki and Pietruszczak (2008). Pietruszczak and Winnicki (2003) described reinforced concrete as a composite medium comprising of a concrete mix and two families of orthogonal reinforcement, and then later Winnicki and Pietruszczak (2008) incorporated the chemo-mechanical ASR interaction in their model. Their suggested model for ASR expansion is heavily based on mathematical formulations, and is thus difficult to implement by practicing engineers.

In the present work, an effective minimalist semi-empirical model is proposed to analyze the expansion strains in reinforced concrete due to ASR expansion over time. The proposed model is then validated using experimental data provided by accelerated laboratory tests as documented in the literature by Hobbs (1988), and Jones and Clark (1996). The results are then discussed and conclusions are drawn.

2.2 The Modeling Approach

The experimental data by Jones and Clark (1996) is shown in Figure 2-1a. It presents the expansion of reinforced cylinder specimens with various reinforcement ratios compared with age. Beyond 200 days, it can be seen that there is a different plateau to the expansion strain for each reinforced concrete specimen; the plateau strain reduces as reinforcement ratio increases. It appears that the rise time for different reinforcement ratios are consistent; in this case, about 40 days.

Based on these two observations, an equation is proposed to estimate the expansion strains in concrete due to ASR effects over time. The general form of the proposed equation is a hyperbolic tangent function and is given in a general form as:

$$\varepsilon(t) = \varepsilon_{\max}(\rho) \tanh\left\langle \frac{t - t_0}{t_r} \right\rangle \tag{2.1}$$

where $\varepsilon(t) =$ the expansion strain in reinforced concrete due to ASR expansion at time t; $\varepsilon_{\max}(\rho) =$ the maximum expansion of concrete which is a function of reinforcement ratio (ρ); $t_0 =$ the time when expansion due to ASR initiates; $t_r =$ the rise time which is the time from the beginning of ASR induced expansion to when the maximum expansion is reached; and $\langle \bullet \rangle$ are the Macaulay brackets which represent a notation used to describe a function, where if $t - t_0 < 0$, then $\frac{t - t_0}{t_r} = 0$.

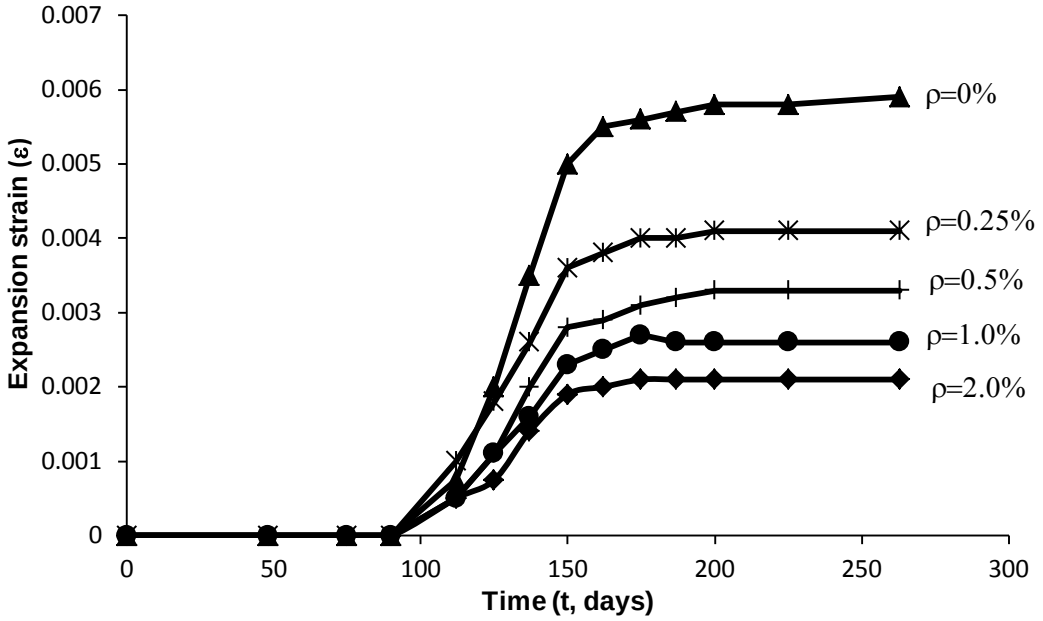

(a)Experimental observation with different reinforcement ratios by Jones and Clark (1996)

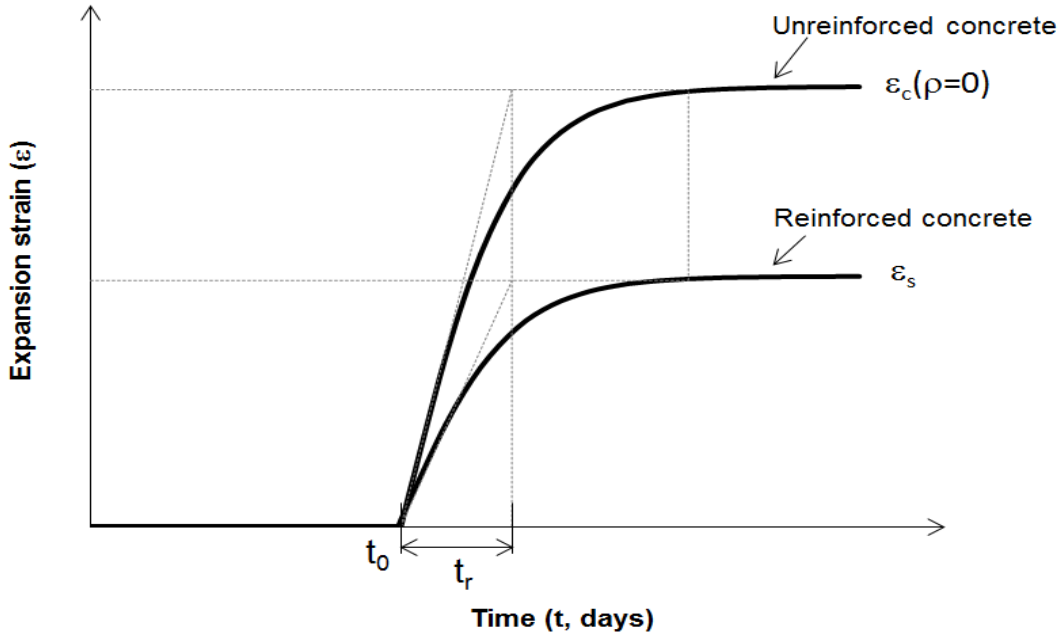

(b)ASR modeling framework

Figure 2-1: Modeling approach for ASR expansion in reinforced concrete.

2.3 Strain Energy Analysis

The strain energy of a member is defined as the energy absorption associated with the deformation of the member. Consider a concrete prism of length L and uniform cross sectional area A, which is attached to a fixed support, and is subjected to an internally generated chemical reaction that causes a swelling force F across the section. Integrating the total work done over the length L gives:

$$U = \int_0^L F dx \tag{2.2}$$

Normalizing over the prism volume to give the strain energy density of the prism leads to:

$$u = \frac{U}{V} = \int_0^L \frac{P dx}{AL} = \int_0^{\varepsilon} \sigma d\varepsilon \tag{2.3}$$

As the concrete swells internally due to the ASR reaction, traction forces are generated, but these are limited to the tensile strength of the concrete $f_t^{'}$. Cracks form, but the concrete matrix finds alternative load path until further cracking forms. Thus, following an initial elastic expansion, a constant state tensile force is maintained across the section as the prism continues to swell lengthwise. Therefore, it is assumed the tensile resistance gives the appearance of being elasto-plastic, as shown in Figure 2-2a. The strain energy density of concrete is given as:

$$u_c = \frac{1}{2} E_c \varepsilon_c^{\,2} - \frac{1}{2} E_c \left\langle \varepsilon_c - \varepsilon_t \right\rangle^2 \tag{2.4}$$

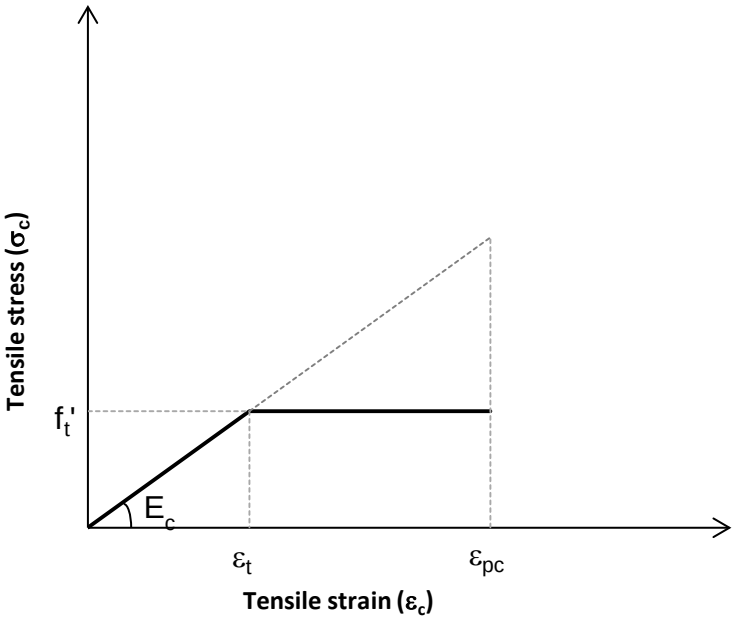

(a)Concrete

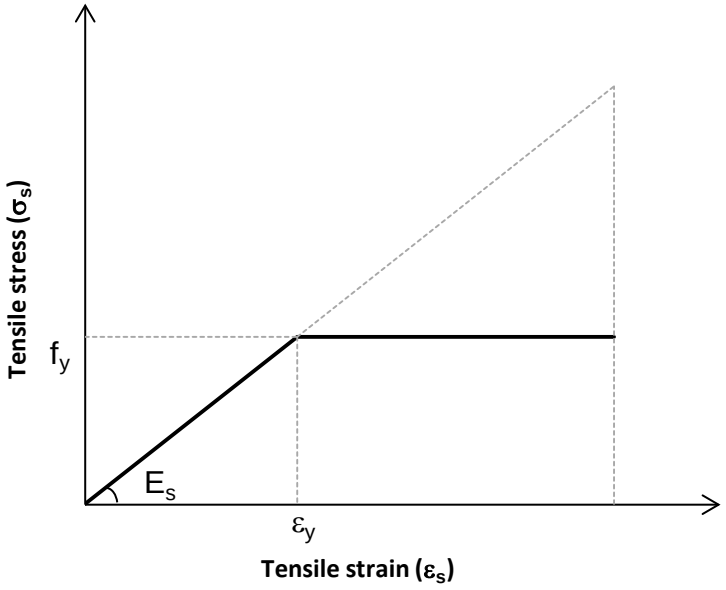

(b)Steel

Figure 2-2: Elasto-plastic stress-strain model.

where E_c = Young's modulus of concrete; ε_c = tensile strain in concrete; and ε_t = the strain corresponding to concrete tensile strength ($f_t^{'}$). Substituting $E_c = f_t^{'} / \varepsilon_t$ and rearranging (2.4) in terms of the total strain energy of concrete (U_C) gives:

$$U_C = f_t^{'} \varepsilon_c \left(1 - \frac{\varepsilon_t}{2\varepsilon_c} \right) A_c L \tag{2.5}$$

Figure 2-2b shows the elasto-plastic stress-strain relationship for steel reinforcement. A general case for calculating the strain energy in the reinforcement is given by:

$$u_s = \frac{1}{2} E_s \varepsilon_s^{\,2} - \frac{1}{2} E_s < \varepsilon_s - \varepsilon_y >^2 \tag{2.6}$$

where E_s = Young's modulus of steel; ε_s = tensile strain in reinforcement. Substituting $E_s = f_y / \varepsilon_y$ in (2.6) and rearranging in terms of total strain energy gives:

$$U_s = \frac{1}{2} E_s \varepsilon_s^{\,2} \left(1 - \left\langle 1 - \frac{f_y}{\varepsilon_s E_s} \right\rangle^2 \right) \rho A_c L \tag{2.7}$$

in which f_y = yield stress of reinforcing steel; ε_y = yield strain of reinforcing steel; ρ = area of reinforcing steel to concrete area ratio ($\rho = A_s / A_c$).

Using the conservation of energy principle, the work done by ASR expansion on plain concrete (U_{PC}) can be equated the work done by ASR expansion on reinforced concrete (U_{RC}).

$$U_{PC} = U_{RC} = U_c + U_s \tag{2.8}$$

where U_c and U_s are given by (2.5) and (2.7), respectively. Due to strain compatibility, it is assumed that the strain in concrete is the same as the strain in the reinforcement that is $\varepsilon_c = \varepsilon_s = \varepsilon_{rc}$. The maximum strain in plain concrete is represented as ε_{pc} (Figure 2-2a). Substituting (2.5) and (2.7) into (2.8) gives the conditional quadratic equation:

$$0 = \frac{1}{2}\rho E_s \varepsilon_{rc}^2 \left(1 - \left\langle 1 - \varepsilon_y / \varepsilon_{rc} \right\rangle^2\right) + f_t \varepsilon_{rc} - f_t \varepsilon_{pc} \tag{2.9}$$

For $\varepsilon_s \geq \varepsilon_y$, when the steel yields, a solution for the tensile strain in reinforced concrete is shown as:

$$\varepsilon_{rc} = \frac{\varepsilon_{pc} + 0.5\varepsilon_y \rho f_y / f_t^{'}}{1 + \rho f_y / f_t^{'}} \tag{2.10}$$

And when $\varepsilon_s < \varepsilon_y$, when the steel does not yield, gives a solution:

$$\varepsilon_{rc} = \frac{f_t^{'}}{\rho E_s}\left(\sqrt{1 + \frac{2\rho E_s \varepsilon_{pc}}{f_t^{'}}} - 1\right) \tag{2.11}$$

Thus (2.10) and (2.11), respectively, are the maximum strains in reinforced concrete when the reinforcement yields and when the reinforcement does not yield ($\varepsilon_{rc} = \varepsilon_{\max}(\rho)$), provided that the maximum strain due to ASR expansion in plain concrete (ε_{pc}) is known.

For large steel volumes when the steel restrains the concrete sufficiently, the reinforcement does not yield, and the expansion strain in reinforced concrete due to ASR expansion is given as:

$$\varepsilon(t) = \left(\sqrt{\left(\frac{f_t^{'}}{\rho E_s} \right)^2 + \frac{2\varepsilon_{pc} f_t^{'}}{\rho E_s}} - \frac{f_t^{'}}{\rho E_s} \right) \tanh \left\langle \frac{t - t_0}{t_r} \right\rangle \tag{2.12}$$

When the steel yields, the expansion strain in reinforced concrete due to ASR expansion is given as:

$$\varepsilon(t) = \frac{\varepsilon_{pc} + 0.5\varepsilon_y \rho f_y / f_t^{'}}{1 + \rho f_y / f_t^{'}} \tanh \left\langle \frac{t - t_0}{t_r} \right\rangle \tag{2.13}$$

For the above two equations, it is evident that this minimalist semi-empirical model needs only knowledge of a few physically measured parameters, specifically: ε_{pc}, f_y, $f_t^{'}$, t_0 and t_r.

2.4 Validation of Proposed Expansion-Time Model

In this section, the proposed minimalist semi-empirical model is calibrated against experimental observations made by Hobbs (1988) and Jones and Clark (1996).

In all the figures presented in this section, the results of numerical simulations are plotted with solid lines, whereas the experimental data are shown using different sets of symbols (circles, triangles, etc.)

The comparison with experimental data from Jones and Clark (1996) is analyzed. The experimental program by Jones and Clark (1996) involved the testing of 180 cylindrical specimens, 100mm in diameter and generally 200mm long. Each test

consisted of four nominally identical cylinders. The cylinders had reinforcement ratios ranging from 0.25% to 2%. The reinforcement was provided as a single bar running down the center of the cylinder. All strains were measured over a 100mm gauge length. Most measurements were carried out using a 100mm DEMEC gauge reading to either 6.75 or 16 microstrain per division. The same gauge was used throughout each test. Figure 2-3 presents the expansion of plain and reinforced cylinder specimens with various reinforcement ratios with time.

From experimental data, the following is evident, $\varepsilon_c = 0.0059$ and $t_r = 39$ days. The following properties for steel and concrete were adopted for a least squares best-fit to the test data, $f_y = 473\ MPa$ and $f_t^{'} = 2.02\ MPa$. Satisfactory agreement is evident between the experimental data and modeled results.

The proposed model is next calibrated against Series I results of Hobbs (1988). The tests were carried out on plain and reinforced concrete specimens and focused on measurements of axial strain caused by the continuing ASR expansion. They were performed at constant ambient conditions with $T = 38^{\circ}C$ and $RH = 100\%$. The water/cement and aggregate/cement ratios were 0.41 and 3, respectively, and reactive particle size was 300~1200 μm. No information on the mechanical properties of concrete ($f_t^{'}$, $f_c^{'}$, E_c) nor the reinforcing steel (f_y, E_s), or the degradation of these properties due to ASR were found in the literature. Figure 2-4a presents the experimental data for Series I specimens, reported by Hobbs (1988).

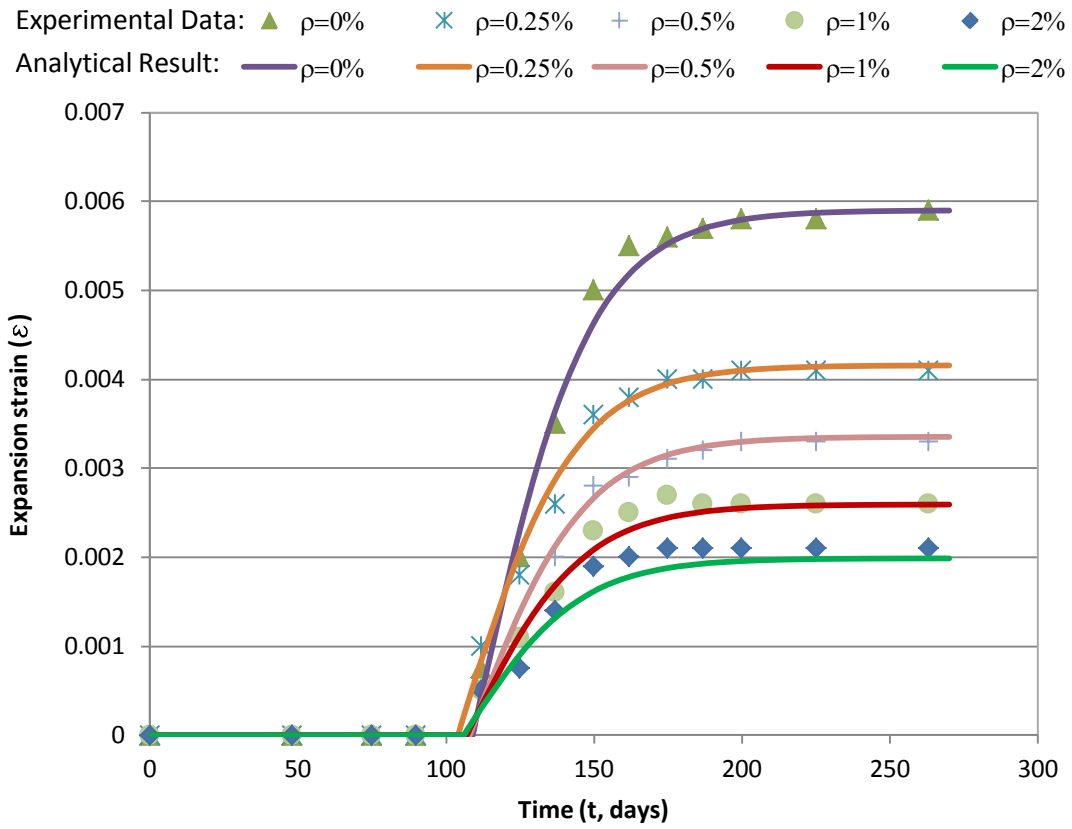

Figure 2-3: Calibration of model with the test results of Jones and Clark (1996).

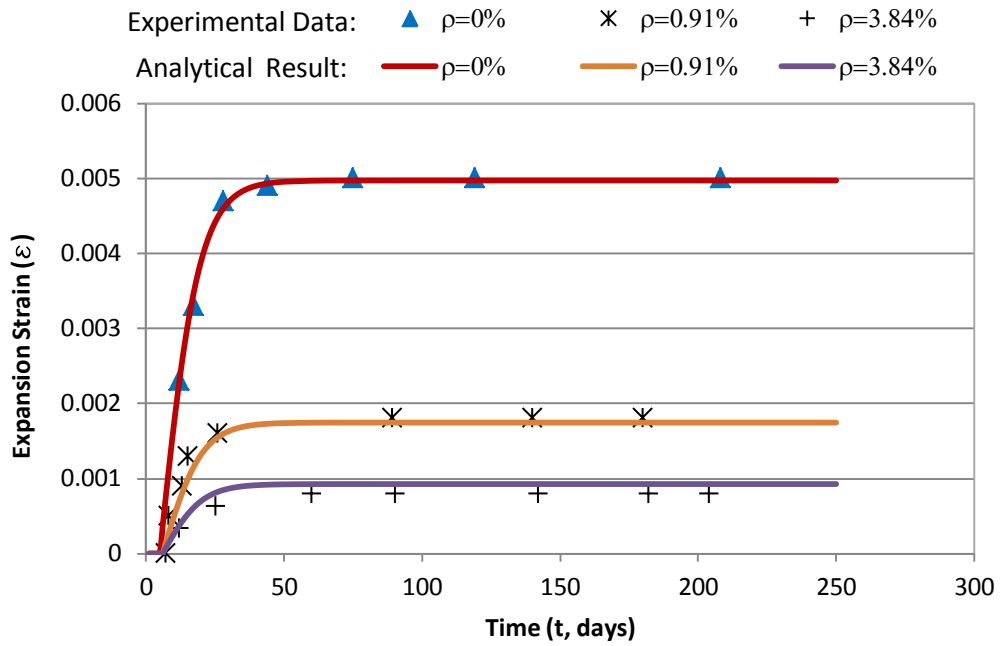

(a) Hobbs (1988) Series I test results vs model

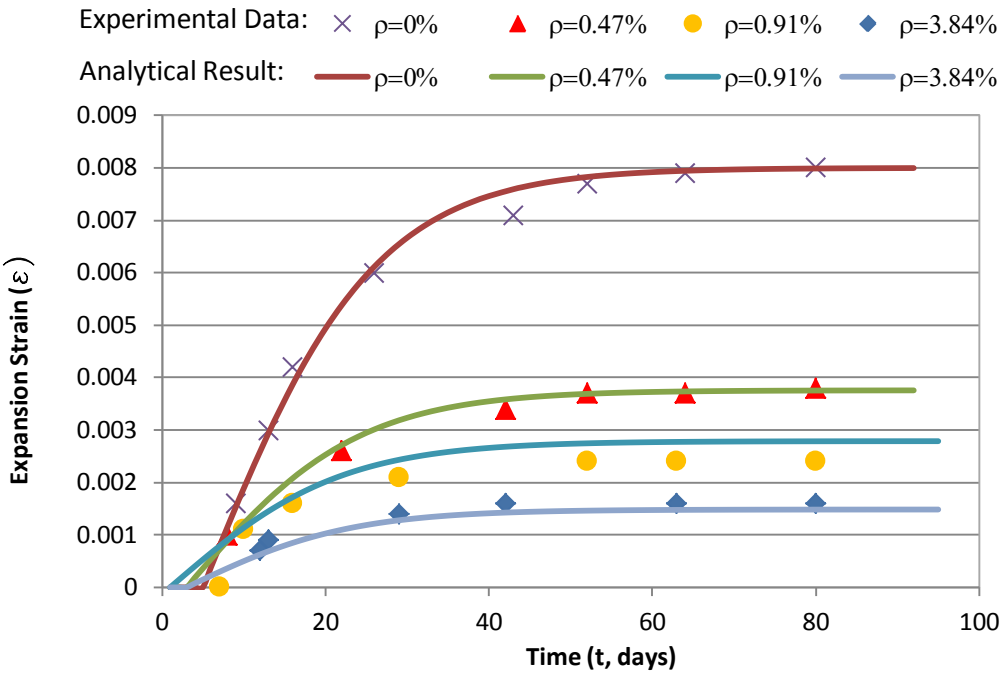

(b) Hobbs (1988) Series II test results vs model

Figure 2-4: Calibration of model with the test results of Hobbs (1988).

From the experimental data, the following is evident, $\varepsilon_c = 0.005$ and $t_r = 14$ days. The following properties for steel and concrete were adopted from a least squares best-fit to the test data, $f_y = 433$ *MPa* and $f_t^{'} = 0.81$ *MPa*. Satisfactory agreement is evident between the experimental data and modeled results.

The proposed model is finally calibrated against Series II results of Hobbs (1988). The Series II tests were carried under similar conditions to Series I, but with one key difference, the reactive particle size was 150~300 μm. Again, no information on the mechanical properties of concrete or steel was provided in Hobbs (1988). Figure 2-4b presents the experimental data for Series II specimens, along with the best-fit modeled results. For the modeling the self-evident experimental results of $\varepsilon_c = 0.008$ and $t_r = 21$ days were adopted and $f_y = 442$ *MPa* and $f_t^{'} = 1.30$ *MPa* were used in the least squares analysis. Again, satisfactory agreement is evident between the experimental data and modeled results.

2.5 Summary and Discussion

A summary of parameters used to obtain the best-fit modeled results for the ASR induced expansion in reinforced concrete are listed in the Table 2-1.

Table 2-1: Parameters used in model to obtain ASR expansion in concrete.

Series	ε_c	t_r (days)	f_y (MPa)	$f_t^{'}$ (MPa)
Jones & Clark (1996)	0.0059	39	473	2.02
Hobbs Series 1 (1988)	0.005	14	433	0.81
Hobbs Series 2 (1988)	0.008	21	442	1.30

The parameter ε_c, which is the maximum unreinforced concrete strain due to ASR expansion and the rise time t_r were obtained from observation of the experimental data. The parameters ε_c and t_r are dependent on several factors such as reactivity of aggregates, the alkalinity of cement, curing condition like temperature and humidity and alkalinity of curing water. The yield strength of steel (f_y) and the tensile strength of concrete ($f_t^{'}$) were obtained by least squares fit of the experimental data. The inferred values of f_y are consistent within the normal range for reinforcing steel. However, the tensile strength of concrete ($f_t^{'}$) shows a wide variation from 0.8 *MPa* to2 *MPa*. The tensile strength for a relatively weak concrete will be roughly 1.5 *MPa*, a value which is somewhat larger than the value inferred from Hobbs tests. However, it should be noted that the rise time is short (either 14 or 21 days) with considerable cracking to be expected in the relatively green concrete prior to the tensile strength fully develops. This

may be a reason for the apparent “weak” tensile strength. However, direct evidence through material tests should be provided in future experimental investigations.

2.6 Closure

The comparison of analytical results with experimental data shown in the previous sections shows that the proposed formulation can give a good estimate of the expansion due to ASR in plain and reinforced concrete. Therefore, the proposed minimalist semi-empirical model is effective and easy to implement for practicing engineers as the model requires only knowledge of the normal material mechanical properties, such as strength and stiffness, the maximum experimental expansion strain and rise time to compute the ASR expansion strain over time. However, the model does not pay attention to the curing environment and detailed chemical mechanism of ASR, which should be further explored.

3. ASR AFFECTED REINFORCED CONCRETE CRACK EVOLUTION

3.1 Introduction

Cracking plays a vital part in the performance of unreinforced and reinforced concrete structures. ASR affects many concrete structures and causes permanent deformation and cracking, which may in turn reduce its durability and structural safety. This section considers the problem of cracking in partly restrained members subjected to direct tension caused by the expansion of ASR gels. The mechanism of cracking due to ASR expansion is discussed. A rational mechanics-based approach is presented for the determination of the number and spacing of cracks. The approach extends to include cracking from the swelling strain theory proposed in section 2. The proposed model is validated with the experimental result by Mander et al. (2012). Predictions agree well with the observed number of cracks.

3.2 Modeling Objective

Using the results described in Mander et al. (2012), Figure 3-1 plots the crack pattern of Specimen 4 of field observations at 48 days, 76 days, 129 days, 176 days, 406 days and 748 days of expansion. The beam is divided into three parts: the beam tension chord edge, the midsection web region and the beam compression chord edge. Only the number of transverse cracks is considered in this section, additional randomly oriented (map) cracking may also exist. The number of cracks counted in each part of the beam over time is plotted in Figure 3-2. A model is proposed to predict the number of cracks and crack spacing in reinforced concrete beam due to ASR gels.

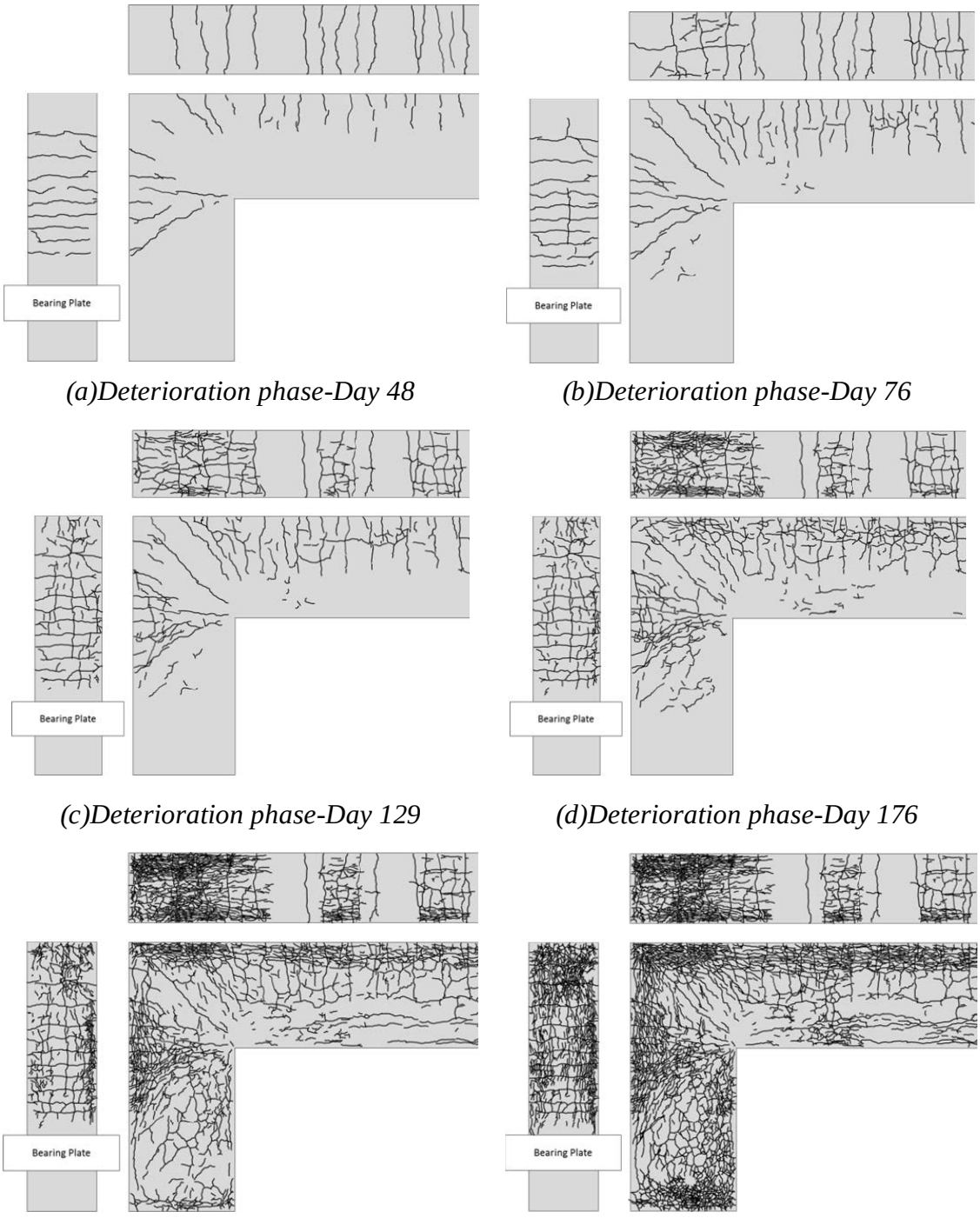

(a)Deterioration phase-Day 48 *(b)Deterioration phase-Day 76*

(c)Deterioration phase-Day 129 *(d)Deterioration phase-Day 176*

(e)Deterioration phase-Day 406 *(f)Deterioration phase-Day 748*

Figure 3-1: Crack patterns observed over time in Specimen 4 (Mander et al. 2012).

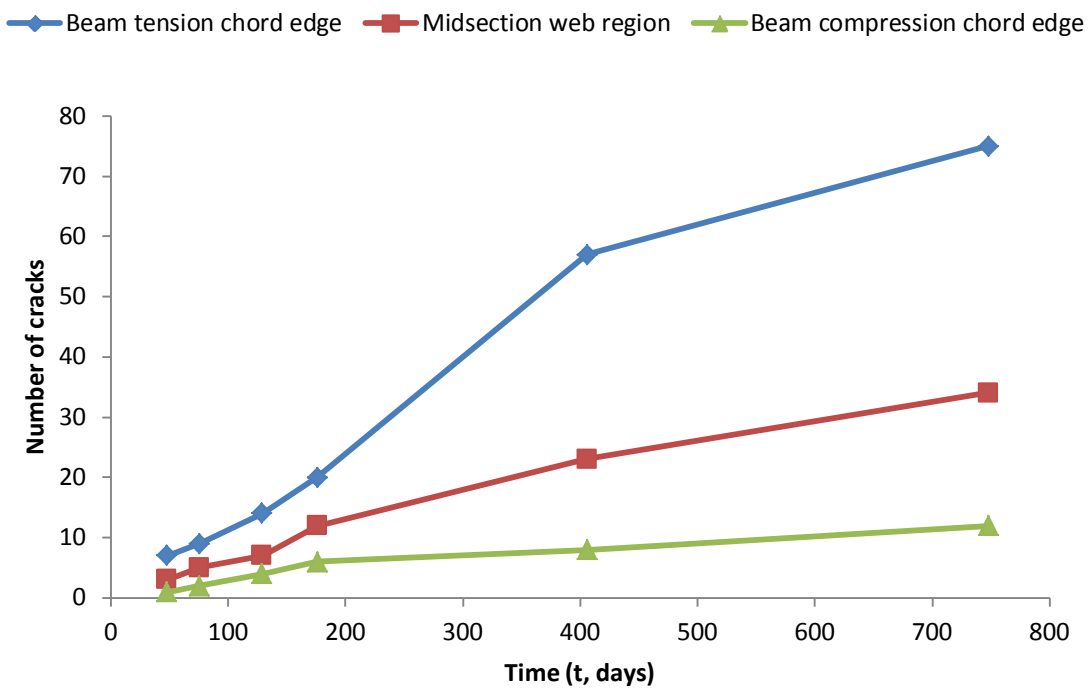

Figure 3-2: The observed number of cracks in different parts of the Specimen 4 beam tested by Mander et al. (2012)

3.3 The Modeling Approach

A rational approach is presented for the determination of the number and spacing of cracks of a reinforced concrete beam, which is partly restrained and subjected only to an axial force caused by the expansion of ASR gels. The approach is based on the principles of mechanics and the swelling strain theory developed in section 2. One assumption has to be made first is that once the force which the ASR gels provide reaches the direct tensile strength of concrete $f_t^{'}$, full-depth direct tension cracking will occur.

3.3.1 First Cracking

A partly restrained reinforced concrete member is considered as shown in Figure 3-3a. As the ASR gel forms and later swells, it starts to push the restrained side of the beam. Once first cracking occurs, the cracking force is given by $N_{cr} = A_c f_t^{'}$, where A_c is the area of concrete, and $f_t^{'}$ is the tensile stress of concrete. The first crack opens to a width (w), as shown in Figure 3-3b. At the crack, the entire axial force is carried by the reinforcement, and the concrete stress is zero. In the region adjacent to the crack, there exists a region of partial bond breakdown where the stresses in concrete and steel vary considerably. At some distance (S) on each side of the crack, the concrete and steel stresses are no longer influenced directly by the presence of the crack (Favre et al, 1983), as shown in Figure 3-3c. As the ASR gel expands and pushes the left side of the reinforced concrete beam, that part of the beam is in compression. The stresses in concrete and steel are shown in Figure 3-3c and d respectively.

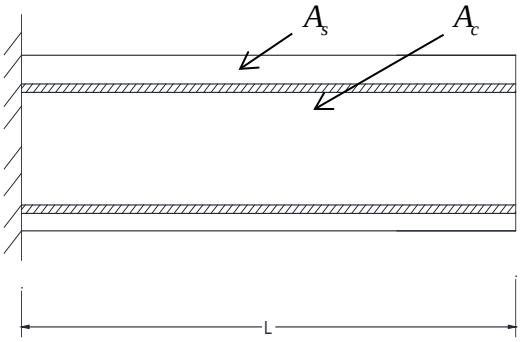

(a) Prior to first crack

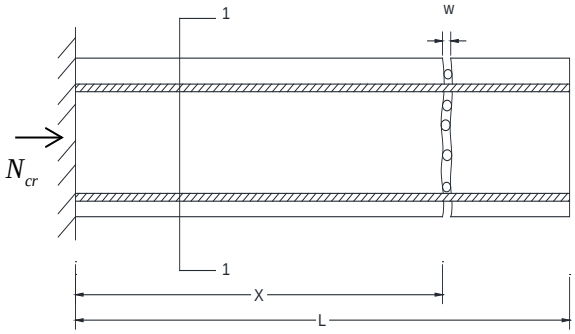

(b) After first crack

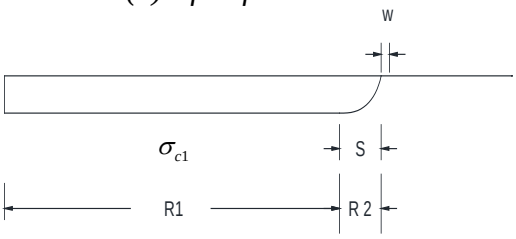

(c) Average concrete stress after first crack

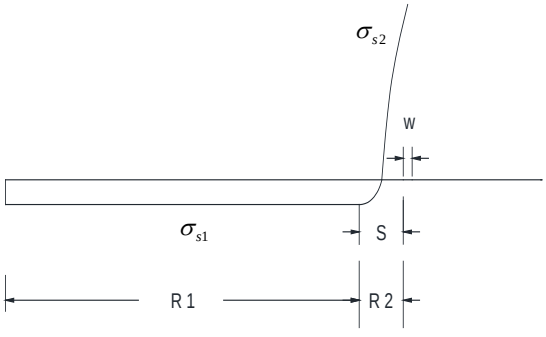

(d) Steel stress after first crack

Figure 3-3: First cracking condition.

The beam under such stress condition is divided to two regions, Region 1 (R1) and Region 2 (R2). R1 is called fully bonded area and R2 is called partly bonded area. In R1, where the distance x from the crack is greater than or equal to *S*, the concrete and steel stresses are σ_{c1} and σ_{s1}, respectively. According to force equilibrium, the sum of the forces in the concrete and steel in this region is equal to cracking force N_{cr}. In R2, where the distance x from the crack is less than *S*, the concrete stress varies from zero at the crack to σ_{c1} at *S*, the steel stress varies from σ_{s2} at the crack to σ_{s1} at *S*, as shown in Figure 3-3c and d respectively.

The distance *S* over which the concrete and steel stress vary, needs to be determined. An approximation for *S* may be obtained using the following equation, which was proposed by Farve et al. (1983) for a member containing deformed bars or welded wire mesh:

$$S = \frac{d_b}{10\rho} \tag{3.1}$$

where d_b = the bar diameter, and ρ = the reinforcement ratio A_s / A_c, where A_s = reinforcement area and A_c = the area of concrete.

The following procedure is used to determine the elongation in the reinforcement at first cracking. In R1, at any distance greater than S from the crack, equilibrium requires that the sum of the forces in the concrete and the steel immediately after first cracking is equal to the cracking force N_{cr}, section 1-1 as shown in in Figure 3-3b is considered, that is:

$$\sigma_{c1}A_c + \sigma_{s1}A_s = -N_{cr} \tag{3.2}$$

In R1, the reinforcement and the concrete work together, therefore strain compatibility is given as follows:

$$\frac{\sigma_{s1}}{E_s} = \frac{\sigma_{c1}}{E_c} \tag{3.3}$$

where, E_s = Young's modulus of steel, E_c = Young's modulus of concrete. By substituting (3.3) into (3.2), the steel stress in R1 is given as:

$$\sigma_{s1} = \frac{-N_{cr}E_s}{(E_cA_c + E_sA_s)} \tag{3.4}$$

Integrating the steel strain over the length of the member, the overall elongation of the steel is given by:

$$\Delta L = \frac{\sigma_{s1}}{E_s}x + \frac{\sigma_{s2} + \sigma_{s1}}{E_s}\left(\frac{1}{3}S + w\right) \tag{3.5}$$

where, $w =$ crack width, as show in Figure 3-3b, c, and d. At the crack, the entire cracking force is carried by the reinforcing steel. That is:

$$\sigma_{s2} = \frac{N_{cr}}{A_s} \tag{3.6}$$

By substituting (3.4) and (3.6) into (3.5), the overall elongation is

$$\Delta L = \frac{-N_{cr}}{\left(E_c A_c + E_s A_s\right)} x + \frac{1}{E_s}\left(\frac{N_{cr}}{A_s} - \frac{N_{cr} E_s}{E_c A_c + E_s A_s}\right)\left(\frac{1}{3}S + w\right) \tag{3.7}$$

Since w is very small compared to S, it can be neglected. The modified overall elongation is given as:

$$\Delta L = \frac{-N_{cr}}{(E_c A_c + E_s A_s)} x + \frac{S}{3E_s}\left(\frac{N_{cr}}{A_s} - \frac{N_{cr} E_s}{E_c A_c + E_s A_s}\right) \tag{3.8}$$

Based on (3.9), an estimate for the elongation of the reinforcement for one crack in the beam can be made.

3.3.2 Final Cracking

Based on the development in the previous section, the following analysis can be used to determine the number of cracks of a reinforced concrete beam due to ASR expansion. Figure 3-4 shows the mechanical analysis of a reinforced concrete beam under the effect of ASR gel expansion. The stress in the reinforcement σ^*_{s2} at the crack in R1 is given by:

$$\sigma^*_{s2} = \frac{N_{cr}}{A_s} \tag{3.9}$$

In R1, at any distance greater than S from the crack, equilibrium requires that the sum of the forces in the concrete and the steel is equal to N_{cr} , that is:

$$\sigma^*_{c1} A_c + \sigma^*_{s1} A_s = -N_{cr} \tag{3.10}$$

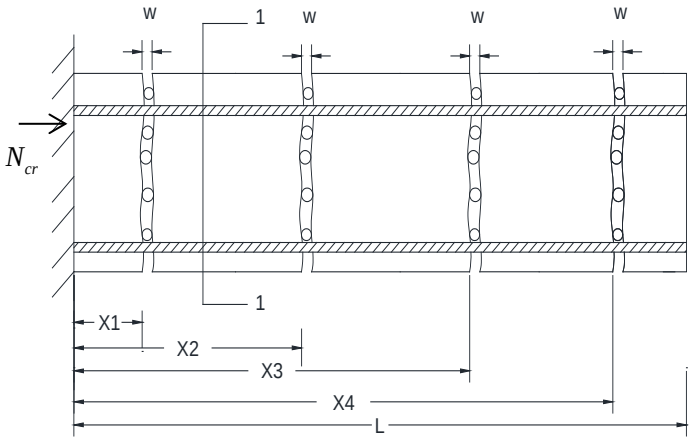

(a). Final cracking condition

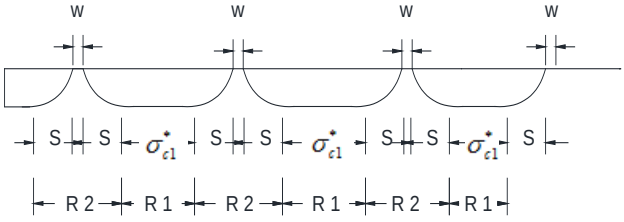

(b). Average concrete stress in the final condition

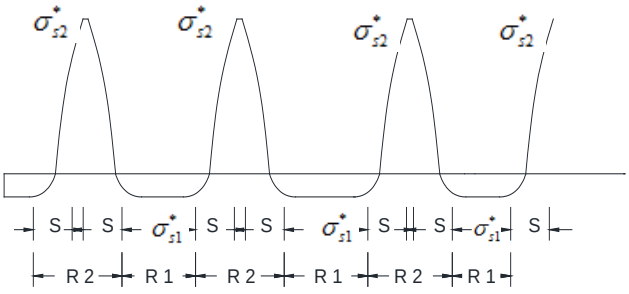

(c). Steel stress in the final condition

Figure 3-4: Final cracking condition.

where σ_{c1}^{*} = concrete stress in R1 in final stage; and σ_{s1}^{*} = steel stress in R1 in final stage. In R1, the reinforcement and the concrete work together and therefore the strain compatibility is given as follows:

$$\frac{\sigma_{s1}^{*}}{E_s} = \frac{\sigma_{c1}^{*}}{E_c} \tag{3.11}$$

Substituting (3.11) into (3.10) gives the steel stress σ_{s1}^{*} in R1 as:

$$\sigma_{s1}^{*} = \frac{-N_{cr}E_s}{(E_c A_c + E_s A_s)} \tag{3.12}$$

Integrating the steel strain over the length of the member gives the overall elongation of the steel

$$\Delta L = \frac{\sigma_{s1}^{*}}{E_s}x_1 + \frac{\sigma_{s1}^{*}}{E_s}(x_2 - x_1) + \frac{\sigma_{s1}^{*}}{E_s}(x_3 - x_2) + \frac{\sigma_{s1}^{*}}{E_s}(x_4 - x_3) + (m-1)\frac{(\sigma_{s2}^{*} + \sigma_{s1}^{*})}{E_s}\left(\frac{2S}{3} + w\right) + \frac{(\sigma_{s2}^{*} + \sigma_{s1}^{*})S}{3E_s} \tag{3.13}$$

where $m =$ the number of cracks. Since w is very small compared to S, it can be neglected. Rearranging terms gives:

$$\Delta L = \frac{\sigma_{s1}^{*}}{E_s}x_4 + \frac{2S(m-1)}{3E_s}(\sigma_{s2}^{*} + \sigma_{s1}^{*}) + \frac{S}{3E_s}(\sigma_{s2}^{*} + \sigma_{s1}^{*}) \tag{3.14}$$

The original length of the beam is assumed to be L, and when a lot of cracks exist in the beam, x_4 can approximated to the length of the beam L, which gives the strain in the reinforcement ε_s as:

$$\varepsilon_s = \frac{\sigma_{s1}^*}{E_s} + \frac{2S(m-1)}{3E_sL}\left(\sigma_{s2}^* + \sigma_{s1}^*\right) + \frac{S}{3E_sL}\left(\sigma_{s2}^* + \sigma_{s1}^*\right) \tag{3.15}$$

It is seen that strain of the reinforcement ε_s and number of cracks m are varying over time. Substituting (3.1) in (3.5), the total number of cracks over time may be estimated with respect to the length L under consideration:

$$\frac{m(t)}{L} = \frac{15\rho}{d_b}\left(\frac{E_s\varepsilon_s(t) - \sigma_{s1}^*}{\sigma_{s1}^* + \sigma_{s2}^*}\right) \tag{3.16}$$

Following section 2, the strain of reinforcement is the strain of reinforced concrete analyzed, that is $\varepsilon_s(t) = \varepsilon(t)$, two solutions are possible depending on the quantity of reinforcement steel present: for large steel volumes when the steel restrains the concrete sufficiently, the reinforcement does not yield:

$$\varepsilon(t) = \left(\sqrt{\left(\frac{f_t^{'}}{\rho E_s}\right)^2 + \frac{2\varepsilon_c f_t^{'}}{\rho E_s}} - \frac{f_t^{'}}{\rho E_s}\right)\tanh\left\langle\frac{t-t_0}{t_r}\right\rangle \tag{3.17}$$

and when the steel yields:

$$\varepsilon(t) = \frac{\varepsilon_c + 0.5\varepsilon_y\rho f_y / f_t^{'}}{1 + \rho f_y / f_t^{'}}\tanh\left\langle\frac{t-t_0}{t_r}\right\rangle \tag{3.18}$$

It should be noted that in (3.16), $\varepsilon(t)$ has a limit equal to the yield strain of the steel. Over time, once the steel yields, instead of an abundance of new cracks forming, rather, the cracks that have formed merely grow wider as the steel will continue to yield within the crack. Equation (3.16) thus gives a maximum number of cracks per length L, as follows:

$$\frac{m_{\max}}{L} = \frac{15\rho}{d_b}\left(\frac{f_y - \sigma_{s1}^*}{\sigma_{s1}^* + \sigma_{s2}^*}\right) \tag{3.19}$$

In the calibration of section 2, it was shown that when $\rho < 0.01$, it may be assumed that reinforcement will yield, thus (3.18) is used to calculate the number of crack; whereas, when $\rho > 0.02$, it may be assumed that the reinforcement will not yield, thus (3.17) is used to calculate the number of cracks. For other cases, both equations (3.17) and (3.18) need to be considered.

Based on the equation of the number of crack per meter over time, crack spacing s_m over length L can be formed as follows:

$$s_m(t) = \frac{L}{m(t)} \tag{3.20}$$

where, s_m and L are in any consistent units.

3.4 Numerical Examples

In the experiment by Mander et al. (2012), the following material properties are adopted: $E_s = 200000\ MPa$; $E_c = 25000\ MPa$; $f_t^{'} = 2\ MPa$; $\varepsilon_y = 0.0022$; $f_y = 440\ MPa$ and $d_b = 25\ mm$. For ASR parameters, the maximum expansion strain of plain concrete due to ASR expansion is assumed to be $\varepsilon_c = 0.005$, initial time is seen to be $t_0 = 40$ days and partial saturation occurs in the concrete for 5% of the time leads to a rise time of 2 year, that is $t_r = 730$ days.

The number of cracks with different reinforcement ratios is plotted in Figure 3-5a, the dash line is the maximum number of cracks based on (3.19). The graph of the

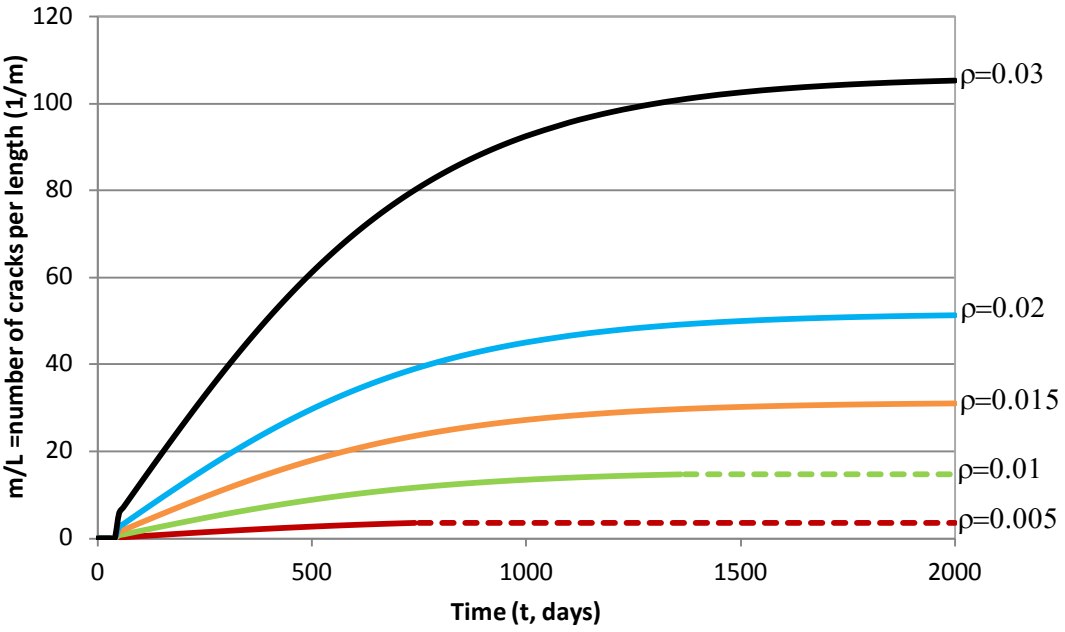

(a) Number of cracks per meter length over time and maximum numbers

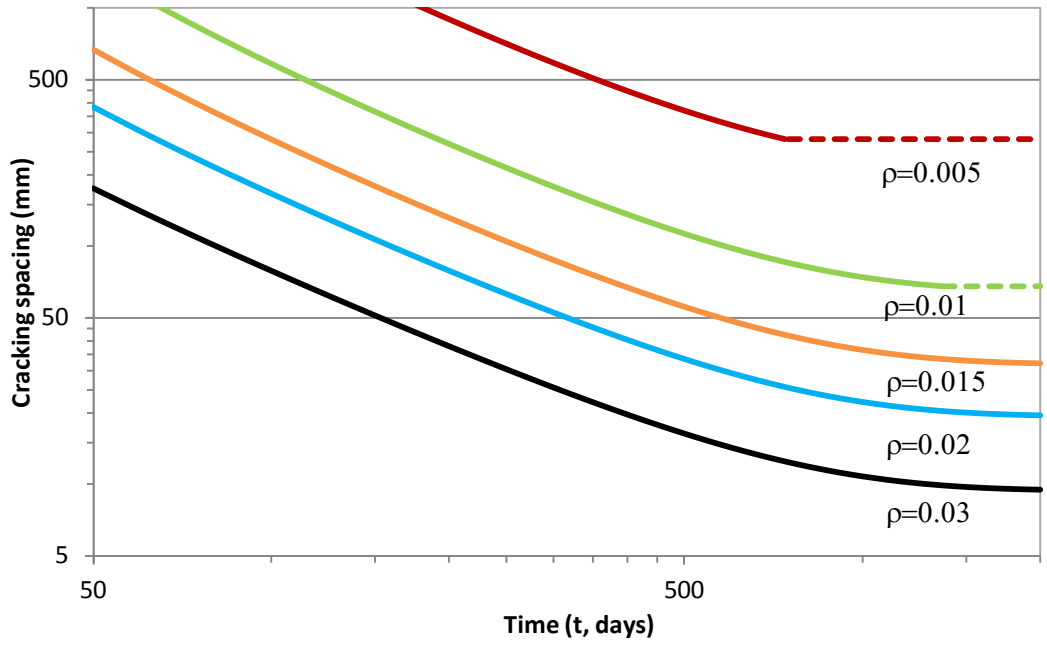

(b) Crack spacing of long reinforced concrete members

Figure 3-5: The effect of cracking on reinforced concrete elements affected by ASR induced swelling strains.

Note: Solid curves show steel has not yield and dash lines show that steel has yielded

log of crack spacing as a function of the log of time with different reinforcement ratios is plotted in Figure 3-5b.

3.5 Validation with the Results of Mander et al. (2012)

In this section, the proposed model is calibrated against cracking condition of the beam tension side edge of Specimen 4 observed by Mander et al. (2012). The specimen represents typical modern Texas reinforced concrete bridge piers. The detailed information about the specimen is described in section 1. The reinforcement ratio in the tension side edge is around 2% and length of tension edge is 1.83 *m*. The number of cracks per meter length is compared with the model result as shown in Figure 3-6. Satisfactory agreement is evident between them.

3.6 Key Findings in This Section

The followings are some key findings in this section:

i. The number of cracks and crack spacing of a reinforced concrete beam due to ASR expansion is dependent on the amount of reinforcement. With higher reinforcement, more cracks and smaller crack spacing occur, and with lower reinforcement, less cracks but wider crack spacing may be expected. Once the steel yields, the number of cracks eventually remains the same; the cracks that have formed merely grow wider as the steel will continue to yield between the crack faces.

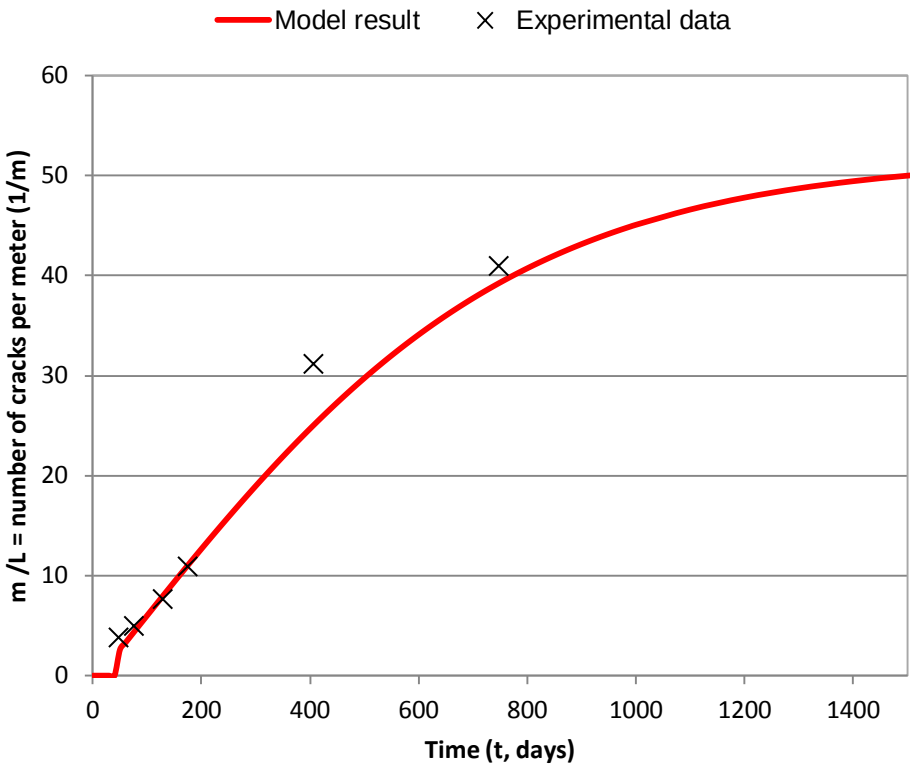

Figure 3-6: Comparison of model with the test results of Mander et al. (2012).

ii. The comparison of the modeled results with experimental data shown in the previous section shows that the proposed formulation can give a good estimate of the number of cracks of a reinforced concrete beam due to ASR expansion. However, the analysis is based on a simplified model as shown in Figure 3-3 and Figure 3-4, the assumption is that full-depth cracking will occur immediately once the force which the ASR gels reach the tensile strength of concrete $f_t^{'}$. In reality, ASR may initially exist at the concrete surface and later with the occurrence of cracks, and may propagate further due to moisture penetration. This aspect should be further considered in the future advancement of model.

iii. The number of cracks and crack spacing are heavily related with crack width. Crack width may influence the number of cracks or crack spacing with different reinforcement ratios. Therefore, the crack width needs to be investigated in the future.

4. SUMMARY, CONCLUSIONS, AND RECOMMENDATIONS

4.1 Summary

This study was primarily concerned about modeling the influence of ASR expansion on reinforced concrete structures. A minimalist semi-empirical model was developed to represent the degradation of reinforced concrete due to ASR expansion. The model was then validated using historical experimental data. Only two key parameters were needed to represent the expansive behavior, specifically, the maximum unreinforced concrete strain due to ASR expansion and the rise time. Mechanical properties of the constituent materials of reinforced concrete were also needed.

From the predicted expansions, it was then shown that it was possible to model the number and spacing of cracks of a partly restrained reinforced concrete beam affected by ASR gels. The model was validated with recent experimental results on large scale reinforced concrete specimens. Predictions agreed well with the observed number of cracks.

4.2 Conclusions

Based on this research, the following conclusions are drawn:

i. The minimalist semi-empirical model well represents the strain expansion due to ASR behavior within reinforced concrete elements over time.

ii. The strain expansion behavior is controlled by just a few parameters. The extent of ASR expansion in plain (unreinforced) concrete (ε_c) is governed by the aggregate chemistry as well as the rise time (t_r) under saturated conditions.

iii. For reinforced concrete, the total expansion strain (ε) is restrained by the amount of reinforcing steel (ρ), along with the steel yield stress and strain, and the tensile cracking strain of concrete under direct tension ($f_t^{'}$) The rise time (t_r) for reinforced concrete due to ASR expansion is evidently invariant to the amount of steel (ρ).

iv. The number of cracks and crack spacing of a reinforced concrete beam due to ASR expansion is also dependent on the amount of reinforcement. With higher reinforcement, more cracks and smaller crack spacing occur, and with lower reinforcement, less cracks but wider crack spacing may be expected. Once the steel yield, the number of cracks remains the same.

v. A rational mechanics-based approach developed for the determination of number of cracks in a reinforced concrete beam due to ASR expansion shows promising results for large-scale specimens.

4.3 Recommendations

Further work needs to be done to ensure the model is complete and robust in the future. The following are some recommendations that can be investigated as a continuation of this research.

i. The influence of several factors such as reactivity of aggregates, the alkalinity of cement, curing condition like temperature, humidity and degree of saturation of the post-hardened concrete that may affect the rise time (t_r) and the pH of the

curing water on the maximum unreinforced concrete strain due to ASR expansion (ε_{cp}) should all be investigated further.

ii. Tests on the degradation of material property affected by ASR gels, especially the yield strength of steel f_y and the tensile strength of concrete $f_t^{'}$ should be investigated.

iii. Experimental investigation on crack width of reinforced concrete beam due to ASR expansion over time needs to be further studied.

iv. It is believed that the model is also valid for DEF expansion. But this needs comprehensive validation for both plain (unreinforced) concrete, as well as reinforced concrete structures.

REFERENCES

Bazănt, Z.P., and Steffens, A. (2000). "Mathematical model for kinetics of alkali-silica reaction in concrete." *Cement and Concrete Research,* 20, 419-428.

Blanks, R.F. (1941). "Concrete deterioration at Parker Dam." *Engineering News-Record,* 126, 462-465.

Comi, C., Beatrice, K., and Rossella, P. (2012). "Two-phase damage modeling of concrete affected by alkaili-silica reaction under variable temperature and humidity conditions." *International Journal of Solids and Structures,* 49, 3367-3380.

Comi, C., Fedele, R., and Perego, U. (2009). "A chemo-thermo-damage model for the analysis of concrete dam affected by alkali-silica reaction." *Mechanics of Materials*, 41(3), 210-230.

Dent, G.L.S. (1979). "Osmotic pressure and the swelling of gels." *Cement and Concrete Research*, 9(4), 515-517.

Dent, G.L.S., and Kataoka, N. (1981). "The chemistry of alkali aggregate reaction." *Cement and Concrete Research*, 11(1), 1-9.

Fan, S.F., and Hanson, J.M. (1998). "Length expansion and cracking of plain and reinforced concrete prisms due to alkali-silica reaction." *ACI Material Journal*, 95, 480-487.

Farve, R., Koprna, M., and Radojivic, A. (1983). *Manuel du CEB*, Comite euro-international du beton, Lausanne, Switzerland.

Hansen, W.C. (1944). “Studies relating to the mechanism by which the alkali-aggregate reaction produces expansion in concrete.” *Journal of the American Concrete Institute*, 15, 213-227.

Hobbs, D.W. (1988). *Alkali-silica reaction in concrete,* Thomas Telford, London, UK.

Jensen, V. (2004). “Alkali-silica reaction damage to Elgeseter Bridge, Trondheim, Norway: a review of construction, research and repair up to 2003.” *Materials Characterization*, 53, 155-170.

Jones, A.E.K., and Clark, L.A. (1996). “The effects of restraint on ASR expansion of reinforced concrete.” *Magazine of Concrete Research*, 48(174), 1-13.

Li, K., and Coussy, O., and Eymard, R. (1999). “Concrete ASR degradation: From material modeling to structure assessment.” *Concrete Science and Engineering*, 4(13), 35-46.

Mander, J.B., Bracci, J.M., Hurlebaus, S., Grasley, Z.C., Karthik, M.M., Liu, S., and Scott, R.M. (2012). “Structural Assessment of "D" Regions Affected by Premature Concrete Deterioration: Technical Report.” *Report. No. FHWA/TX-12/0-5997-1,* Texas A&M Transportation Institute, The Texas A&M University System, College Station.

Meissner, H.S. (1941). “Cracking in concrete due to expansion reaction between aggregate and high-alkali cement as evidenced in Parker Dam.” *Proceedings of American Concrete Institute*, 37, 549-568.

Mukhopadhyay, A.K., Shon, C.S., and Zollinger, D.G. (2006). "Activation energy of alkali-silica reaction and dilatometer method." *Journal of the Transportation Research Board*, 1-11.

Multon, A., Seignol, A.F., and Toutlemonde, F. (2006). "Chemomechanical assessment of beams damaged by alkali-silica reaction." *Journal of Materials in Civil Engineering*, 18, 500-509.

Pietruszczak, S., and Winnicki, A. (2003). "Constitutive model for concrete with embedded sets of reinforcement." *Journal of Engineering Mechanics*, 129(7), 725-738.

Santon, T.H. (1940). "Expansion of concrete through reaction between cement and aggregate." *Proceedings of American Society of Civil Engineers*, 66, 1781-1811.

Saouma, V., and Perotti, L. (2006). "Constitutive model for alkali-aggregate reactions." *ACI Materials Journal*, 103, 194-202.

Swamy, R.N., and Al-Asali, M.M. (1989). "Effect of alkali-silica reaction on the structural behavior of reinforced concrete beams." *ACI Materials Journal*, 86, 451-459.

Tarig, A., Eldon, B., Stephen, R., and Abid, I. (2003). "The effect of alkali reactivity on the mechanical properties of concrete." *Construction and Building Materials*, 17, 123-144.

Ulm, F., Coussy, O., Kefei, L., and Larive, C. (2000). "Thermo-Chemo-Mechanics of ASR Expansion in Concrete Structures." *Journal of Engineering Mechanics*, 126(3), 233-242.

Winnicki, A., and Pietruszczak, S. (2008). “On mechanical degradation of reinforced concrete affected by Alkali-Silica Reaction.” *Journal of Engineering Mechanics*, 134(8), 611-627.